Pergamon

PII: S0022-3697(98)00008-0

J. Phys. Chem Solids Vol 59, No. 9, pp. 1639–1645, 1998
0022-3697/98/$ - see front matter
© 1998 Elsevier Science Ltd. All rights reserved

GROWTH STUDIES OF THIN FILMS OF $BaTiO_3$ USING FLASH EVAPORATION

R. A. ZÁRATE[a], A. L. CABRERA[a,*], U. G. VOLKMANN[a] and V. FUENZALIDA[b]

[a]Facultad de Física, Pontificia Universidad Católica de Chile de Casilla 306, Santiago 22, Santiago, Chile
[b]Facultad de Ciencias Físicas y Matemáticas, Universidad de Chile, Casilla 487-3, Santiago, Chile

(*Received* 28 *August* 1997; *accepted* 7 *December* 1997)

Abstract—A flash evaporation technique was implemented to grow polycrystalline thin films of $BaTiO_3$ onto Si(100) substrates, which were prepared with protective layers of SiO_2 or Pt/TiW. X-ray diffraction and X-ray photoelectron spectroscopy studies of the films suggest the formation of $BaTiO_3$ with good stoichiometry and with a tetragonal crystal structure phase for a given set of growth parameters. The inspection of the films under scanning electron microscopy revealed that the topography and morphology depended strongly on the type of the protective layers. Grain sizes smaller than 0.1 μm were found for films deposited on the SiO_2 layer and around 1 μm for films on top Pt/TiW layers. Preliminary studies of the dielectric properties of the films grown onto Pt/TiW show that the dielectric loss varied from 0.01 to 0.1 and the dielectric constant varied from 8 to 75 at 1 kHz. The electrical resistivity varied from 10^{12} to 10^{13} Ω-cm and the breakdown electric field had values from 180 to 1000 kV/cm for these films. © 1998 Elsevier Science Ltd. All rights reserved

1. INTRODUCTION

A number of ceramic class of materials have been extensively studied because of their very interesting properties, such as ferroelectricity, piezoelectricity, piroelectricity, elastic, optics and electro-optics properties [1]. These materials in the form of thin films have been used in a wide variety of practical applications. Devices such as dielectric barrier layers [2], ultrasonic tranducers [3], electro-optic modulators/switches [4], surface acoustic wave devices [5], piroelectric infrared detectors [6] and memory devices [7] have been produced.

In particular, the major area of applicability of ferroelectric materials is in digital memory devices, such as dynamic random access memory (DRAM) and ferroelectric random access memory [8]. $BaTiO_3$ is an attractive compound for these applications because of its high values of dielectric constant and breakdown electric field. The thin films of $BaTiO_3$ are promising materials for being the best storage dielectric for the future in ultra-large-scale integrated memory devices [9].

The most common processes used for synthesis of $BaTiO_3$ films are rf sputtering [9–13], vacuum evaporation [14, 15], laser ablation [16, 17], metallo-organic chemical vapor deposition [18, 19], sol-gel [20], metallo-organic decomposition [21] and hydrothermal processes [22, 23]. These techniques have been sucessfully used to grow thin films of $BaTiO_3$ and other ferroelectric compounds onto several substrates. However, the integration of the thin films in the silicon technology have been hampered, mainly, due to its poor performance compared to bulk material [7]. In addition, some techniques require expensive and complicated equipment, especially molecular beam epitaxy [1].

Although there has been considerable progress in electronic devices at present, many problems which appear in the fabrication of thin films are far from being completely solved, such as stresses, stoichiometry and contamination. Such problems not only influence the properties of thin films but also could affect the reliability of electronic devices made from thin films [24]. A typical problem that has been extensively studied is the interdiffusion at high temperature of some components of the ferroelectric material into the silicon wafers. The heat treament at high temperature causes several problems, such as degraded interfaces and a rough surface morphology. In other words, the electrical characteristic of the thin films degrade [13]. Initially, the thin films were directly deposited onto the silicon and this caused severe interdiffusion [11, 18, 19]. An alternative solution was investigated: putting buffer layers between ferroelectric material and silicon [9, 10, 13, 17, 20] such as insulating or metallic material. For capacitors and field effect transistors, the most common buffer layers used have been Pt, Pt/Ti, SiO_2, Ti, Pt/Ti/SiO_2, Pt/SiO_2, RuO_2, Pd, CeO_2 and CaF_2. Recently, Suzuki and Ami [25] proposed studying the properties of ferroelectric thin films grown onto conductive perovkites, such as $SrRuO_3$.

*Corresponding author.

In this present work we report the making of the thin films of $BaTiO_3$ (from 30 to 300 nm) on a Si(100) substrate with protective layers of SiO_2 or Pt/TiW using a simple and inexpensive method called flash or discrete evaporation. We used both buffer layers in order to compare crystallinity and the dielectric characteristics of the films grown. This technique produced thin films with good dielectric properties, they all exhibited a high resistivity (between 10^{12} and $10^{13}\,\Omega$-cm) through the films.

This method consists of dropping a small portion of base material, grain by grain, into a heater that is at a high temperature. Each grain evaporates suddenly and completely before the next one arrives. This technique was used for the first time by Müller *et al*. [26]. They wanted to avoid the fabrication of films of no homogeneous structure, such as the films that Feldman [14] fabricated. Some work was carried out successfully using this technique to evaporate alloys, such as cadmium telluride [27, 28], superconducting ceramics [29], and barium titanate [30–34], among others.

2. EXPERIMENTAL METHOD

We prepared flash-evaporated $BaTiO_3$ films with thicknesses varying from 30 to 300 nm. This method was implemented in an Edwards Auto 306 system, which was modified specially for the application of this technique (Fig. 1). More details of this technique are found elsewhere [33].

The substrates used for the growth of the thin films were arsenic-doped silicon wafers, [100] oriented, n type, degenerated, 1–3 mΩ-cm. Some of the substrates contained 100 nm of thermally grown SiO_2, and the others contained 100 nm of platinum evaporated by sputtering. The latter contained 100 nm of TiW between the Si-surface and the Pt-film, in order to avoid the formation of the platinum silicide and favor the formation of titanium silicide in treatments at high temperature. All the substrates were cleaned in the following way: first, they were washed with methanol (analytical quality) in an ultrasonic bath, and then they were heated at high temperature in the vacuum chamber before evaporation.

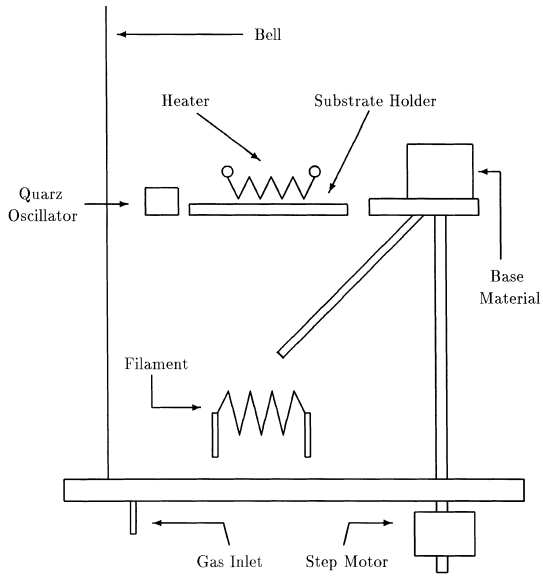

Fig. 1. Schematic diagram of the system for growing flash evaporated films. The step motor is energized with a square wave of variable frequency.

The evaporation conditions used in the modified Edwards system were similar to those used by others investigators [26, 30]. We heated the substrate at different temperatures between 450 and 720°C. The typical growth rate average was 8–40 Å/min. This rate was controlled by a step motor of variable frequency. The particles of $BaTiO_3$ fell through a hole of 500 μm diameter and the size of particles was chosen between mesh 100 and 200 (nominal diameters of 150 and 75 μm). The base pressure of the chamber was 1.0×10^{-6} mbar. The oxygen pressure was increased by admitting air into the chamber up to a pressure ranging from 3.0×10^{-6} to 1.0×10^{-3} mbar. The tungsten boat temperature was typically between 1700 and 1800°C.

The crystal structures of the films were determined by X-ray diffraction (XRD). All XRD spectra were taken at room temperature with a Siemens D5000 Diffractometer using a CuKα source and couple 2θ–θ scan. Also, we took additional XRD spectra at grazing incidence for the films grown onto substrates covered with a Pt-layer. The spectra of these films in the 2θ–θ scan show very intense lines corresponding to silicides formed by the reaction of the protective layers with the silicon which hinder the lines of the perovskite $BaTiO_3$. The morphology of the films was examined with scanning electron microscopy (SEM) using a Joel JSM-5300 with detector for secondary and back-scattered electrons. The electron beam can be accelerated at voltages in the range of 1–30 kV.

XPS spectra were obtained for determining the elemental composition of the films and the presence of contamination. X-ray photoelectron spectroscopy (XPS) was performed with a Perkin Elmer model 1257 hemispheric analyzer using AlKα radiation ($h\nu = 1486.6$ eV). All XPS spectra at high and low resolution were taken at room temperature. The electric properties of the films were analyzed using metal–oxide–metal (MOM) and metal–oxide–SiO_2–nSi–metal (MOIS) structures. The structures were made by evaporating gold or silver dots with 0.5 mm diameter and 200 nm thickness on the films. For the MOIS structures a Pt-layer was deposited on the silicon side for good electric contact. Physical evaporation was used for making these electric contacts. We used a Keithley 595 Quasistatic Meter for obtaining I–V characteristics and an SI 1260 Impedance/Gain-phase

Analyzer for obtaining dielectric characteristics as a function of the frequency.

3. RESULTS AND DISCUSION

The crystal structure of the flash-evaporated thin films varied, mainly, depending on substrate temperature, oxygen partial pressure, the growth rate and the W-boat temperature.

The thin films deposited with the W-boat at a temperature equal or lower than 1700°C contained a mixed phase of $BaTiO_3$ and $BaCO_3$. The formation of a carbonate is the result of the excess of barium oxide which is caused by keeping the W-boat temperature near the melting point of titanium oxide, titanium metallic or $BaTiO_3$ compound. On the other hand, when the W-boat was at a temperature greater than 1700°C, the films contained only phases of the perovskite $BaTiO_3$, as indicated by XRD patterns. However, undesirable tungsten oxide could be present in the films at these temperatures that when the boat was kept below 1700°C. Curves (a) and (b) of Fig. 2 show XRD spectra corresponding to films fabricated with W-boat at a temperature of 1700 and 1800°C onto SiO_2 layers, respectively; the lines marked with BC, in Fig. 2, correspond to the $BaCO_3$ compound.

The crystallinity of the films versus substrate temperature has been extensively studied by several researchers [18, 26, 30]. They have found that when the substrate temperature is kept over 500°C during the evaporation, the films have better crystallinity. Our films produced with substrate temperatures in the range 530–710°C show only phases of $BaTiO_3$. This is comfirmed by XRD, shown in Figs 2 and 3. Substrate temperature was not important for obtaining $BaTiO_3$ in this range. The differences in XRD patterns corresponding to curves (a), (b) and (c) in Fig. 2 are due to differences in background

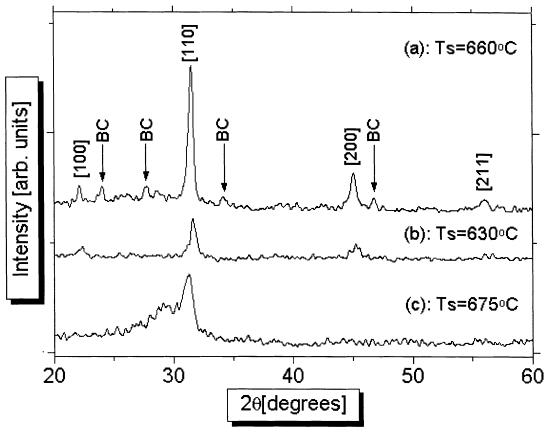

Fig. 2. XRD patterns of the films deposited onto SiO_2 layers (a) with W-boat at 1700°C, (b) W-boat at 1800°C and (c) grown at substrate temperature of 675°C. The lines of thin $BaTiO_3$ film are indicated by their Miller indexes.

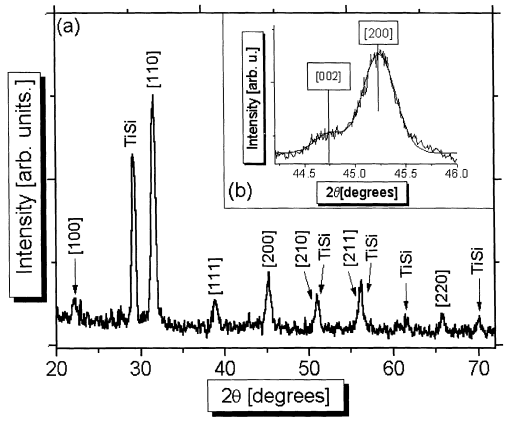

Fig. 3. XRD patterns of the thickest films grown at 630°C on Pt/TiW layers. (a) The lines of the polycrystalline $BaTiO_3$ thin film are indicated by their Miller indexes and (b) the presence of [002] line indicates a marked tetragonal distortion.

pressure and W-boat temperature. Fig. 3 shows a difraction pattern corresponding to a 300 nm film grown at 630°C onto Pt/TiW layers, the lines marked with TiSi corresponding to the reaction of the protective layers with silicon (forming titanium silicide). These lines (TiSi) marked the difference between the XRD patterns corresponding to the different protective layers used; in the SiO_2 case, the XRD patterns show only lines corresponding to the polycrystalline $BaTiO_3$ for the films grown under optimal evaporation conditions (curve (b) in Fig. 2).

Pressures higher than 10^{-4} mbar did not allow the formation of $BaTiO_3$. Curve (c) in Fig. 2 corresponds to XRD of a 30 nm film that was fabricated at 10^{-4} mbar. The XRD pattern shows only the [110] line of the polycrystalline $BaTiO_3$ and a broad line at the left side of this line. This broad line could arise from the formation of an amorphous phase of the film. On the other hand, pressures in the range of 3.0×10^{-6} to 1.0×10^{-4} mbar allowed the formation of polycrystalline $BaTiO_3$. The curve (b) of the Fig. 2 corresponds to a 30 nm film grown at 3.0×10^{-6} mbar. The XRD pattern of curve (b) shows only lines of polycrystalline $BaTiO_3$ and the broad lines corresponding to an amorphous phase are missing.

The films deposited with an average growth rate around 25 Å/min allowed the formation of the perovskite $BaTiO_3$ and values greater than 40 Å/min did not allow it. The term ''average'' means the growth rate is estimated from the final thickness and the time employed for the evaporation. This estimate was done because the flash evaporation is a discrete process.

The tetragonal phase was obtained with both protective layers used, although the tetragonal distortion appears more marked on Pt/TiW layers than on the SiO_2 layer. Fig. 3(b) shows a marked distortion towards tetragonality of a film deposited on Pt/TiW layers. This seems related to the growth dynamics of the grains, a tetragonal distortion of the line [200] could be detected only for large

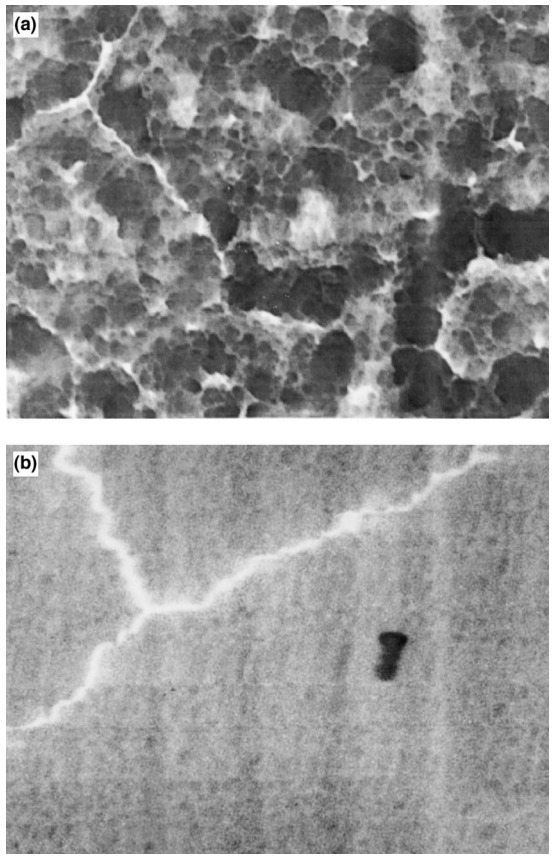

Fig. 4. Scanning electron micrographs of the surface of the thickest $BaTiO_3$ films deposited at 630°C onto (a) Pt/TiW layers and (b) SiO_2 layer.

grains [12]. It was found by scanning electron microscopy that the grain size was around 1 μm for Pt/TiW layers and less than 0.1 μm for SiO_2 layer. The lattice constants for the thin film with tetragonal structure were calculated and they were of 4.00 $\pm$ 0.01 and 4.04 $\pm$ 0.01 Å for Pt/TiW layers and 4.00 $\pm$ 0.01 and 4.03 $\pm$ 0.01 Å for the SiO_2 layer.

Fig. 4(a) shows a micrograph corresponding to a film grown at 630°C onto Pt/TiW layers. The grain size varied between 0.1 and 1 μm and depends on the thicknesses of the films. The topology of these films displays grains agglomerated in large chains of 3–8 μm, each grain touching its neighbor. On the other hand, the micrograph shown in Fig. 4(b) displays a homogeneous surface for the film grown at 630°C onto a SiO_2 layer. It was not possible to see the grain boundaries of this film at this magnification. The best estimate of the grain size is smaller than 0.1 μm.

The chemical composition of all flash-evaporated thin films was identical on the surface and in deeper layers. The detected elements were barium, oxygen, titanium, carbon and tungsten. Fig. 5(a) shows a typical low resolution spectrum showing its principal components. The binding energies for the different elements present on

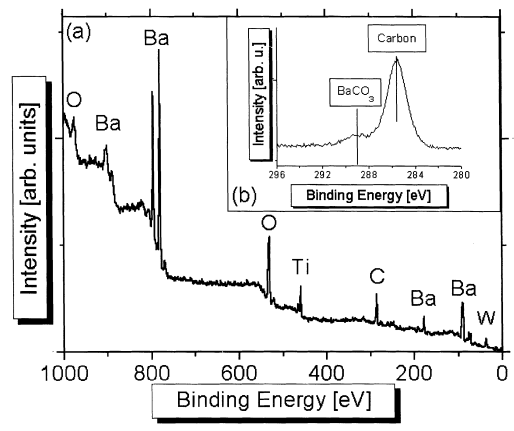

Fig. 5. XPS analysis of a typical flash evaporated $BaTiO_3$ thin film. (a) A low resolution spectrum shows the principal components of the film and (b) the carbon line at high resolution spectrum, which shows the presence of carbon and carbonate before sputtering with argon ions. The line around 70 eV corresponds to Pt.

the surface of the film were: 779.4 eV for $Ba3d_{5/2}$ line, 457.8 eV for $Ti2p_{3/2}$ line and 529.4 eV for O1s line. These values were referred to the carbon signal at 284.6 eV. A comparison of the spectra of a $BaTiO_3$ single crystal and of the flash-evaporated thin films shows that both spectra are identical.

The carbon C1s line shows two components: the higher peak corresponds to a binding energy of 284.6 eV and the smaller, of 288.0 eV. The smaller peak probably corresponds to barium carbonate, located in a thin layer on the surface of the flash-evaporated thin films, as can be seen in Fig. 5(b). Pilleux and Fuenzalida [23] found similar results in $BaTiO_3$ thin films using a hydrothermal process. This layer is the result of a quick reaction of some free BaO with CO_2 when the films were exposed to air. After the films were bombarded with argon ions of 4 kV, the C1s line reduces to a trace level.

Stoichiometry is an important issue in the fabrication of thin films of $BaTiO_3$. For the vacuum technique, a difficulty arises because the evaporation rates of BaO and TiO_2 are different, and it is more difficult to control it for those techniques that use $BaTiO_3$ in powder (flash evaporation) or target (sputtering) than in others which use two targets, such as the electron beam technique [15]. The stoichiometry of the flash-evaporated thin films was estimated from XPS spectra of high and low resolution. This estimate was done with the heights of the peaks of $Ba3d_{5/2}$ and $Ti2p_{3/2}$, the rate Ba/Ti was typically in the range of 1.2–3.0, and the best stoichiometry (closer to 1.0) was found in the thickest film fabricated (300 nm).

All flash-evaporated thin films showed a very small amount of contamination with tungsten oxide. The sources of this contamination might be explained in two different ways. One is the reaction of the oxygen of the

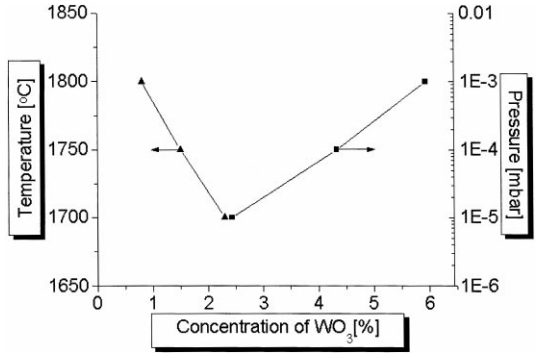

Fig. 6. Tungsten oxide concentration of the $BaTiO_3$ films as a function of total pressure in the chamber and W-boat temperature.

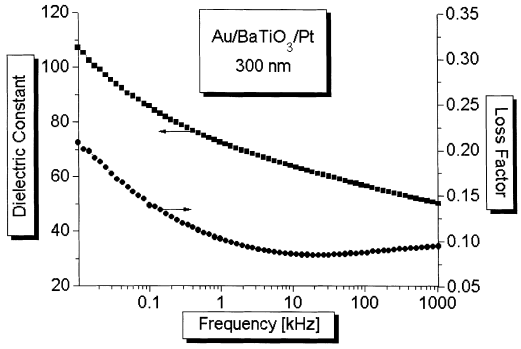

Fig. 7. Frequency dependence of dielectric constant and dielectric loss for the thickest $BaTiO_3$ film grown at 630°C onto Pt/TiW layers.

base material with the W-heater while it is at high temperature during the deposition. The other is the reaction of the oxygen in the chamber directly with the W-heater. The binding energy of the $W4f_{7/2}$ line was 34.8 eV which corresponds to the WO_3 compound. The atomic percentage of tungsten oxide in the films depends more on the increments of the total pressure in the chamber than on the W-boat temperature. In Fig. 6, we plot the amount of W-oxide found in the films as a function of the W-boat temperature during the evaporation and as a function of oxygen pressure in the chamber.

A preliminary study of the dielectric properties of the thin $BaTiO_3$ films deposited on silicon wafers have been carried out after making the MOM structure. The dielectric constant and loss depended strongly on the crystallinity of the films. For films of 30 nm of thickness deposited on Pt/TiW layers, the dielectric constants were 24 and 7.5 and the losses were 0.08 and 0.03, respectively. The differences in the dielectric constant and the loss is explained in the differences in crystallinity of the films: the film with the larger dielectric constant is more crystalline than the other film. Diffraction patterns corresponding to these films are similar to the pattern shows in Fig. 3.

For the same properties, the thickest films fabricated simultaneously on Pt/TiW layers with differences in the substrate temperature show differences in their dielectric constants. The film made with the hotter substrate temperature had a dielectric constant around 75 and a loss of 0.1, the other film had a dielectric constant of around 50 and a loss of 0.01. The crystallinity obtained by XRD spectra was better for hotter substrates. Fig. 7 shows the dielectric constant and the loss as a function of frequency for the thickest film grown onto Pt/TiW layers.

The dielectric constant for films on SiO_2 layers was estimated from the metal–oxide–SiO_2–nSi–metal (MOIS) and metal–SiO_2–nSi–metal (MIS) structures. The oxide layer forms a capacitor which is in series with the capacitor of $BaTiO_3$. Assuming the capacitors are perfectly parallel (without interdiffusion) and the capacitor area is the same as that defined by the top electric contacts, the estimate can be carried out measuring the impedance of two structures as a function of the frequency. This type of estimate was done by Li and Lu [36] for MOIS capacitors with an ultra-thin layer of SiO_2. In this present work, the dielectric constant for the MIS structure was independent of the frequency in the range of 100 Hz to 1 MHz and the value of the capacity was 90.2 pF. On the other hand, in the MOIS structure, the capacity varied with the frequency. The value estimated for the dielectric constant for $BaTiO_3$ was of 200 at 1 kHz and it was 108 at 1 MHz. The estimated values of the dielectric constant for the films deposited onto SiO_2 layers was greater than the films grown onto Pt/TiW layers.

XRD patterns show that the intensity of the peaks corresponding to $BaTiO_3$ in films grown onto the SiO_2 layer was larger than those films deposited on Pt/TiW layers. This could indicate that the films grown on SiO_2 are more crystalline than films deposited on Pt/TiW layers. However, the Pt/TiW layers scatter the X-ray more than the SiO_2 layer due to the high atomic number of platinum and tungsten.

A ferroelectric behavior was found in a 0.03 μm film grown at 630°C onto Pt/TiW layers. A Saywer–Tower [35] modified circuit operating at 1 kHz was used to measure this property. Fig. 8 shows a hysteresis loop for this sample, which had a nonsaturating P–E relationship. The remnant polarization is 0.65 $\mu C/cm^2$, the coercive field was 250 kV/cm. Similar results were obtained by Lee and Park [18]. This kind of nonsaturating loop had been observed by Slack and Burfoot [31] and Paniz and Hu [10], who based the nonsaturating behavior on complex processes of conduction due to the contamination of the film. Lee and Park [18] proposed that the nonsaturating loop came from the diffuse layer between $BaTiO_3$ and silicon. In the present work, the nonsaturating behavior probably came from the nonhomogeneous surfaces in films grown onto Pt/TiW layers. The top electrode (Au or Ag) could be located on grains of $BaTiO_3$ (over chains

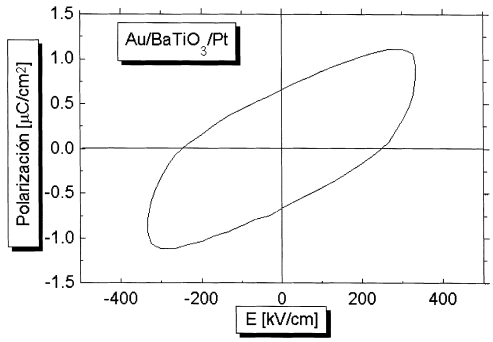

Fig. 8. Polarization hysteresis behavior of the thinnest $BaTiO_3$ film deposited at 630°C onto Pt/TiW layers.

and grains without nucleation) and amorphous materials (see Fig. 4(a)).

The complex processes of conduction were confirmed by the *I–V* characteristics at high electric field for the ferroelectric film. Fig. 9 shows the *I–V* characteristic corresponding to ferroelectric film and the insert in this figure shows the *I–V* curve corresponding to low electric field. The backward bias was similar to the forward bias, i.e. the characteristic is symmetric. It indicates the absence of the any Schottky barrier in the interface of the $BaTiO_3$ and electric contact. The change of slope of the *I–V* characteristic in the forward bias indicates the onset of a space-charge controlled conduction process [17]. This was the only process of conduction which we could identify. Detailed studies are in progress for understanding the conduction mechanisms in flash-evaporated thin $BaTiO_3$ films.

The electric resistivity was also calculated from the *I–V* characteristics. In the ohmic region, the resistivity was as high as 10^{12}–10^{13} Ω-cm for the films grown onto Pt/TiW layers. The breakdown field was estimated using the *I–V* characteristic and Saywer–Tower circuit. In the thickest and in the thinnest film grown onto Pt/TiW layers, the breakdown field was around 180 and 1000 kV/cm, respectively.

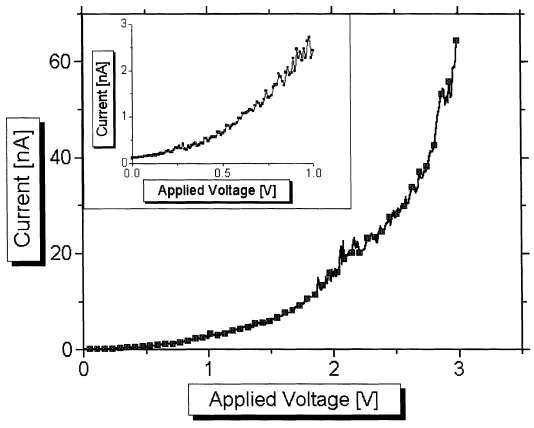

Fig. 9. *I–V* characteristic for the thinnest $BaTiO_3$ film deposited at 630°C onto Pt/TiW layers.

4. CONCLUDING REMARKS

Polycrystalline thin $BaTiO_3$ films have been fabricated on silicon substrate by a flash evaporation technique. Under optimal evaporation conditions (substrate temperature between 530 and 630°C, growth rate average around 25 Å/min, total presure in the chamber from 3.0×10^{-6} to 2.0×10^{-5} mbar and W-boat temperature around 1800°C), we grew thin films of $BaTiO_3$ with a good stoichiometry and ferroelectric phase.

The discrete process used for growing the films influenced the crystallinity of the films because they had an amorphous component too. The crystalline phase is responsible for the high dielectric constant (75 and 200 at 1 kHz) and the amorphous phase for the high electric resistivity (around 10^{13} Ω-cm). The result obtained using the flash evaporation technique is very important, because the films with a high crystallinity tend to have high electrical conductivity [13]. The films with a dielectric constant between 100 and 200, which have a homogeneous surface and an electrical resistivity as high as 10^{13} Ω-cm, are preferred for dynamic random access memory (DRAM) [24].

The *P–E* hysteresis loops at 1 kHz and the XRD spectra demonstrated that the ferroelectricity is present in the films. A complex process of conduction was confirmed by the *I–V* characteristics and space charge limit conduction.

The deposition rate was one of the parameters most difficult to control. The reason was that during the growth of the films, the base material agglomerated around the hole obstructing the passage of this material toward the boat; sometimes this eventually stopped the films growth.

Acknowledgements—This work was partially supported by grants from FONDECYT No. 2950066 and No. 4950016. We gratefully acknowledge the use of facilities in the Facultad de Ciencias Biológicas, Pontificia Universidad Católica de Chile and Comisión Chilena de Energía Nuclear, La Reina. Surface analysis facilities were provided by Fundación Andes under grants c10810-2 and c12510. The authors wish to express their sincere thanks to Dr. Oscar Wittke and Judit Lisoni for stimulating discussion about XRD patterns. We also acknowledge the assistance of José Ampuero for obtaining the XRD spectra, José Morillas for obtaining the micrographs and R. Avila for obtaining the dielectric properties of the films.

REFERENCES

1. Yuhuan Xu, *Ferroelectric Materials and Their Applications*. North-Holland, Elsevier Science Publishers B.V., 1991.
2. Sayer, M. and Sreenivas, K., *Sciences*, 1990, **247**, 1056.
3. Mansingh, A., *Ferrolectrics*, 1990, **102**, 69.
4. Glass, A. M., *Sciences*, 1987, **235**, 1003.
5. Castellans, R. N. and Feinstein, L. G., *J. Appl. Phys.*, 1979, **50**, 4406.
6. Beerman, H. P., *Ferroelectrics*, 1971, **2**, 123.
7. Haertling, G. H., *J. Vac. Sci. Technol. A.*, 1991, **9 (3)**, 414.
8. Scott, J. F. and Paz de Araujo, C. A., *Sciences*, 1989, **246**, 1400.

9. Desu, S. B., *Phys. Stat. Sol. (a)*, 1994, **141**, 119.
10. Paniz, J. K. G. and Hu, C. C., *J. Vac. Sci. Technol.*, 1979, **12 (2)**, 315.
11. Dharmaghikari, V. D. and Grannemann, W. W., *J. Appl. Phys.*, 1982, **53 (12)**, 8988.
12. Schäfer, H., Schmitt, H., Ehses, K. H. and Kleer, G., *Ferroelectrics*, 1978, **22**, 775.
13. Jia, Q. X., Shi, Z. Q. and Anderson, W. A., *Thin Solids Films*, 1992, **209**, 230.
14. Feldman, C., *Review of Scientific Instruments*, 1955, **26 (5)**, 463.
15. Iijima, K., Terashima, T., Yamamoto, K., Hirata, K. and Bando, Y., *Appl. Phys. Lett.*, 1990, **56 (6)**, 527.
16. Davis, G. M. and Gower, M. C., *Appl. Phys. Lett.*, 1989, **55 (2)**, 112.
17. Roy, D. and Krupanidhi, S. B., *Appl. Phys. Lett.*, 1992, **61 (17)**, 2057.
18. Lee, C. H. and Park, S. J., *Journal of Materials Science: Material in Electronics*, 1990, **1**, 219.
19. Kim, T. W., Yoon, Y. S., Yom, S. S. and Kim, C. O., *Appl. Surface Sci.* , 1995, **90**, 75–80.
20. Frey, M. H. and Payne, D. A., *Appl. Lett.*, 1993, **63 (20)**, 2753.
21. Xu, J. J., Shaikh, A. S. and Vest, G. M., *IEEE Transaction on UltrasonicFerroelectrics, and Frequency Control*, 1989, **36 (3)**, 307.
22. Yoo, S. E., Yoshimura, M. and Somiya, S., *J. Mater. Sci. Lett.*, 1989, **8**, 530.
23. Pilleux, M. E. and Fuenzalida, V., *J. Appl. Phys.*, 1993, **74 (7)**, 4664–4672.
24. Petrovsky, V. I., Sigov, A. S. and Vorotilov, K. A., *Integrated Ferroelectric*, 1993, **3**, 59.
25. Suzuki, M. and Ami, T., *Materials Science and Engineering*, 1996, **B41**, 166–173.
26. Müller, E. K., Nicholson, B. J. and Francombe, M. M., *Electrochem. Technol.*, 1963, **1**, 158.
27. Menezes, C. A., *Electrochem. Soc.*, 1980, **127**, 155.
28. Felix-Valdés, J., Falcomy, C., Tufino, U. and Menezes, C., *Rev. Mexicana Fis.*, 1987, **33**, 583.
29. Hatou, J., Takai, Y. and Hayakawa, *Jpn J. Appl. Phys.*, 1988, **27**, L617.
30. Slack, J. R. and Burfoot, J. C., *Thin Solid Film*, 1970, **6**, 233.
31. Slack, J. R. and Burfoot, J. C., *J. Physics C. St. Phys.*, 1971, **4**, 898.
32. Tomashpolskii, Y. Y. and Sevost'yanov, M. A., *Sov. Phys. Crystallogr.*, 1975, **19 (5)**, 644.
33. N. Beltrán, V. Fuenzalida and C. Grahmann, in *Eurocera-mics II, Electroceramics and ceramics for special applica-tions*, Vol. 3, ed. G. Ziegler and Husner. Deutche Keramische Gesellschaft, 1989, pp. 2424–2429.
34. Fuenzalida, V., Beltrán, N., Grahmann, C. and Perez, M., *J. Vac. Sci. Technol. A.* **7**(6), Nov/Dec 1989, 3205.
35. Sawyer, C. B. and Tower, C. H., *Phys. Rev.*, 1930, **35**, 269.
36. Li, P. and Lu, T. M., *Appl. Phys. Lett.*, 1990, **57 (22)**, 2336.